Applied Thermal Engineering 81 (2015) 74–82

Contents lists available at ScienceDirect

Applied Thermal Engineering

journal homepage: www.elsevier.com/locate/apthermeng

Research paper

Non-equilibrium condensation of wet steam flow within high-pressure thermo-compressor

S.M.A. Noori Rahim Abadi, R. Kouhikamali*, K. Atashkari

Department of Mechanical Engineering, Faculty of Engineering, University of Guilan, Rasht, Iran

HIGHLIGHTS

- With the increase of motive steam pressure the mass fraction of liquid phase increases.
- The effects of slip velocity become more important in high-pressure motive steam.
- During condensation liquid temperature become larger than that of vapor phase.
- The second nucleation phenomenon occurs at the mixing region of thermo-compressor.
- Droplet production in secondary nucleation process in larger than that of primary one.

ARTICLE INFO

Article history:
Received 2 November 2014
Accepted 10 February 2015
Available online 18 February 2015

Keywords:
Two-fluid model
Supersonic flow
High-pressure thermo-compressor
Non-equilibrium condensation

ABSTRACT

In this study unsteady supersonic flow of wet steam through high-pressure thermo-compressor with non-equilibrium homogeneous condensation has been presented. Two-fluid multiphase flow formulations are applied for the simulation of unsteady, supersonic and compressible flow of wet steam. Non-equilibrium homogeneous condensation of we steam flow with considering suitable equations of state for both vapor and liquid is simulated via in-house CFD code. Results have shown that the proposed two-fluid multiphase approach can predict the non-equilibrium condensation of wet steam within high-pressure thermo-compressor. Quantitative validations of the calculated parameters with industrial data are presented. The validation of the in-house CFD code proves its usefulness for the modeling of steam condensing flows within high-pressure thermo-compressors which are very practical in desalination industry.

1. Introduction

Thermal vapor compressors (TVC) are the essential parts of the multi-effect desalination (MED) systems. TVCs simply consist of a supersonic primary nozzle, a mixing chamber and a diffuser. They boost the lower pressure steam to a high pressure by using the supersonic flow of the motive steam passing through the primary nozzle. Improving the efficiency of TVC can affect the overall performance of MED systems [1]. During the expansion of motive steam through the nozzle a non-equilibrium condensation happens, which results in change in performance of thermo-compressor [2,3]. Computational Fluid Dynamics (CFD) can be used to explain the flow characteristics inside the thermo-compressor with the minimum cost and time. In addition, accurate numerical simulation of thermo-compressor in order to evaluate its performance can improve the efficiency in desalination industry.

Numerical modeling of wet steam spontaneous condensing flow within thermo-compressors, nozzles and turbine cascades is categorized into three types: particle trajectory model, single-fluid model and two-fluid model. In particle trajectory model, the diffusion of liquid phase is ignored but the effect of slip velocity between two phases is considered [4]. In single-fluid model, the effect of slip velocity between vapor and liquid phases is ignored and volume-averaged properties for the mixture of two phases are applied. In two-fluid model, two separate governing equations for each phase are solved. Therefore, the effects of temperature difference, condensation and turbulence interactions and slip velocity are considered. Two-fluid model for the simulation of wet steam spontaneous condensing flow is much more

* Corresponding author. Tel.: +98 131 6690276; fax: +98 131 6690273.
E-mail address: kouhikamali@guilan.ac.ir (R. Kouhikamali).

http://dx.doi.org/10.1016/j.applthermaleng.2015.02.023
1359-4311/

complicated than the other models and consequently much less popular [5].

Numerous studies are performed to investigate the wet steam flow within nozzles, thermo-compressors and turbine cascades with non-equilibrium condensation considering nucleation and droplet growth process based on the mentioned models [6–11]. Dykas and Wroblewski [12] proposed a two-fluid model for the simulation of non-equilibrium condensing steam within low-pressure turbine cascade. They observed the slip velocity between vapor and liquid phases which proved the utilized drag formulations. Ding et al. [13] studied the non-equilibrium condensation of wet steam in sonic nozzle. They present a multi-fluid turbulence model for to investigate the effect of vapor condensation on mass flow-rate of sonic nozzle. The results showed good agreement with thermal choking theory. Avetissian et al. [14,15] investigated the effect of turbulence modeling on non-equilibrium condensation steam through nozzle. They found that the traditional standard k-ε turbulence model is invalid for the simulation of mentioned condensation phenomenon. They also have proposed the modified k-ε turbulence model which could predict the pressure and droplets radius distributions along the nozzle, successfully. Dykas and Wroblewski [16] used single-fluid (SFM) and two-fluid (TFM) models for prediction of steam condensing flow in low-pressure nozzles. They found that TFM can better predict the pressure and droplets radius distributions along the nozzles. Feng-ming et al. [17] proposed a dual-fluid model for the simulation of 2D and nozzle and steam turbine cascade. Their results showed the slip velocity between vapor and liquid phases does not affect the significantly in low-pressure nozzle and cascade. CUI et al. [18] developed the proposed dual-model of Feng-ming et al. [17] for the simulation of non-equilibrium steam condensing flow within 2D Laval nozzles. They found that the effect of condensation on total pressure loss (about 8.78%) is much more than slip velocity (about 0.42%).

Literature reviews show that, all investigations focused on non-equilibrium condensation of wet steam within low and medium pressure thermo-compressors in which the volume fraction of the liquid phase can be neglected. In high-pressure thermo-compressors ($P_{motive\ steam} = 30–50$ bar) the mass fraction of produced liquid phase become large and hence the volume of the secondary phase cannot be neglected. Therefore, a two-fluid model has to be applied, in which all phase-interactions between the phases should to be taken into account. In this study, two-fluid formulation is adopted to predict the non-equilibrium condensation of high-pressure wet steam within industrial thermo-compressor.

2. Physical model

In this study, full Navier stokes equations are solved using an in-house CFD code. The governing equations should to be solved for each phases, separately. The governing equations for the vapor phase are as follows:

$$\frac{\partial(\rho_v(1-\alpha))}{\partial t}+\frac{\partial(\rho_v(1-\alpha)u_{vj})}{\partial x_j}=-(\Gamma_1+\Gamma_2) \tag{1}$$

$$\frac{\partial(\rho_v(1-\alpha)u_{vi})}{\partial t}+\frac{\partial\left(\rho_v(1-\alpha)u_{vj}u_{vi}+(1-\alpha)p_v\delta_{ij}\right)}{\partial x_j}-\frac{\partial((1-\alpha)\tau_{ij})}{\partial x_j}=-(\Gamma_1+\Gamma_2)u_{inti}-F_{Di}-p_{int}\frac{\partial\alpha}{\partial x_i} \tag{2}$$

$$\frac{\partial(\rho_v(1-\alpha)E_v)}{\partial t}+\frac{\partial\left(\rho_v(1-\alpha)u_{vj}H_v\right)}{\partial x_j}+\frac{\partial\left((1-\alpha)q_{vj}-(1-\alpha)u_{vj}\tau_{ij}\right)}{\partial x_j}=-(\Gamma_1+\Gamma_2)(H_{int_v}-h_{l_v})-p_{int}u_{inti}\frac{\partial\alpha}{\partial x_i}-u_{inti}F_{Di} \tag{3}$$

where:

$$E_v=h_v-\frac{p}{\rho_v}+\frac{1}{2}u_{vj}u_{vj} \tag{4}$$

The indices v, l, i and j stand for vapor phase, liquid phase, horizontal and vertical coordinates, respectively. The interface parameters are computed as follows:

$$u_{inti}=\frac{\rho_l u_{li}\alpha+\rho_v u_{vi}(1-\alpha)}{\alpha\rho_l+(1-\alpha)\rho_v} \tag{5}$$

$$H_{int\ v}=h_{v\ sat}+u_{int\ j}u_{vj}-\frac{1}{2}u_{vj}u_{vj} \tag{6}$$

Also P_{int} is the pressure at the interface of liquid and vapor phases. The governing equations for the liquid phase are also defined as follows:

$$\frac{\partial(\rho_l\alpha)}{\partial t}+\frac{\partial\left(\rho_l\alpha u_{lj}\right)}{\partial x_j}=\Gamma_1+\Gamma_2 \tag{7}$$

$$\frac{\partial(\rho_l\alpha u_{li})}{\partial t}+\frac{\partial\left(\rho_l\alpha u_{lj}u_{li}+\alpha p_l\delta_{ij}\right)}{\partial x_j}-\frac{\partial(\alpha\tau_{ij})}{\partial x_j}=(\Gamma_1+\Gamma_2)u_{inti}-F_{Di}-p_{int}\frac{\partial\alpha}{\partial x_i} \tag{8}$$

$$\frac{\partial(\rho_l\alpha E_l)}{\partial t}+\frac{\partial\left(\rho_l\alpha u_{lj}H_l\right)}{\partial x_j}+\frac{\partial\left(\alpha q_{lj}-\alpha u_{lj}\tau_{ij}\right)}{\partial x_j}=(\Gamma_1+\Gamma_2)H_{intl}-p_{int}u_{inti}\frac{\partial\alpha}{\partial x_i}-u_{inti}F_{Di} \tag{9}$$

where:

$$H_{int\ l}=h_{l\ sat}+u_{int\ j}u_{lj}-\frac{1}{2}u_{lj}u_{lj} \tag{10}$$

$$E_l=h_l-\frac{p}{\rho_l}+\frac{1}{2}u_{lj}u_{lj} \tag{11}$$

The drag force between two phases is defined as follows [16]:

$$F_{Di}=\frac{4.5\frac{\mu_l\alpha}{r^2}}{C_c}(u_{vi}-u_{li}) \tag{12}$$

where C_c is Cunningham correction factor [16]:

$$C_c=1+2\,Kn\left(1.257+0.4e^{-1.1/2Kn}\right) \tag{13}$$

The Knudsen number (Kn) is the ratio of the mean free path $\bar{l}$ of vapor molecules to the droplet diameter:

$$Kn=\frac{\bar{l}}{2r} \tag{14}$$

For simplicity, it is assumed that the two phases have the same averaged pressure:

$$P = P_v = P_l \tag{15}$$

Single-pressure method in two-fluid multiphase flow formulations is valid when the gravitational force is negligible [12].

In this study, two-equation turbulence model is applied for each vapor and liquid phases, separately. The equations of turbulence energy and dissipation rate are represented as follows [14]:

$$\frac{\partial(\alpha_q\rho_q k_q)}{\partial t} + \frac{\partial(\alpha_q\rho_q u_{qj} k_q)}{\partial x_j} = \frac{\partial}{\partial x_j}\left(\alpha_q \mu_{qk}\frac{\partial k_q}{\partial x_j}\right) + \alpha_q \tau_{Tij}\frac{\partial u_{qi}}{\partial x_j} - \alpha_q\rho_q\varepsilon_q \tag{16}$$

$$\frac{\partial(\alpha_q\rho_q \varepsilon_q)}{\partial t} + \frac{\partial(\alpha_q\rho_q u_{qj} \varepsilon_q)}{\partial x_j} = \frac{\partial}{\partial x_j}\left(\alpha_q \mu_{q\varepsilon}\frac{\partial \varepsilon_q}{\partial x_j}\right) + \alpha_q\frac{\varepsilon_q}{k_q}\left(C_{\varepsilon 1}\tau_{Tij}\frac{\partial u_{qi}}{\partial x_j} - C_{\varepsilon 2}\rho_q\varepsilon_q\right) \tag{17}$$

where index q stands for vapor or liquid phases. The stress tensor τ_{Tij} is defined as follows:

$$\tau_{Tij} = (\mu_L + \mu_T)\left(\frac{\partial u_{qi}}{\partial x_j} + \frac{\partial u_{qi}}{\partial x_j} - \frac{2}{3}\frac{\partial u_{qj}}{\partial x_j}\delta_{ij}\right) - \frac{2}{3}\rho_q k_q \delta_{ij} \tag{18}$$

where μ_L and μ_T are laminar and turbulent viscosities, respectively. Details of the various parameters and constants used in the turbulence model are given in Refs. [19–21].

The most accurate and widely used equation of state for steam in industrial applications is the IAPWS-IF97 [22]:

$$\frac{p_v}{RT_v\rho_v} = A(T_v) + B(T_v)\rho_v \tag{19}$$

where A (T_v) and B (T_v) are defined as follows:

$$A(T_v) = a_0 + a_1 T_v + a_2 T_v^2 \tag{20}$$

$$B(T_v) = b_0 + b_1 T_v + b_2 T_v^2 \tag{21}$$

The a_i and b_i (i = 0, 1, 2) are the function of temperature only [22].

While several theories have been proposed for developing the nucleation rate during spontaneous condensation, the two main theories of interest are a classical theory which was first presented by Oswatitsch [23] and a theory developed by Deich et al. [24]. During past years several modifications are performed for nucleation theory. One of most common representation of nucleation rate per unit volume and per unit time (J) is expressed as [25]:

$$J = \frac{q_c}{1+\theta}\frac{\rho_v^2}{\rho_l}\sqrt{\frac{2\sigma}{\pi M^3}}\exp\left(-\frac{3\pi r^{*2}\sigma}{3K_b T_v}\right) \tag{22}$$

where q_c is the condensation coefficient which is generally taken as unity, σ is the liquid surface tension, M is the mass of one molecule, K_b is the Boltzmann constant and θ is a non-isothermal correction factor which is given by the following relation [7]:

$$\theta = \frac{2(\gamma-1)}{(\gamma+1)}\left(\frac{h_{lv}}{RT_v}\right)\left(\frac{h_{lv}}{RT_v} - 0.5\right) \tag{23}$$

where h_{lv} is the latent heat of evaporation at pressure p. According to equilibrium thermodynamics, there is a minimum radius r^* (the critical radius) which must be attained in order to form a stable nucleus from supersaturated vapor. The radius of critical clusters (r^*) according to the mentioned real equation of state has a form [12]:

$$r^* = \frac{2\sigma(T_l)}{\rho_l[f(p_v) - f(p_{sat})] - (p_v - p_{sat})} \tag{24}$$

where:

$$f(p) = \frac{b}{2}\ln p + c - \frac{b}{2}\ln\left(\frac{1+\frac{c}{b}}{1-\frac{c}{b}}\right) \tag{25}$$

$$b = A(T)RT \tag{26}$$

$$c = \left[(A(T)RT)^2 + 4pB(T)RT\right]^{0.5} \tag{27}$$

Due to release of latent heat in condensation phenomenon, the produced droplets become hotter than surrounding vapor. Droplet growth rate are highly affected by heat transfer rate. The Knudsen number plays an important role in the heat transfer coefficient due to the wide range of the radius of the droplets [14]. At the beginning of nucleation process, the formed droplets have very small diameter which results in large Kn number (free-molecular regime). Therefore, the droplet growth rate for this regime is presented by the kinetic Hertz–Knudsen model:

$$\left.\frac{dr}{dt}\right|_{HK} = \frac{h_c}{\rho_l}\frac{p}{\sqrt{2\pi R}}\left(\frac{1}{\sqrt{T_V}} - \frac{1}{\sqrt{T_l}}\right) \tag{28}$$

where h_c is the heat transfer coefficient and calculated as follows [14]:

$$h_c = \frac{\lambda_v}{r(1+3.18Kn)} \tag{29}$$

With increase of droplet radius during droplet growth process the Knudsen number decreases (continuum regimes) and therefore droplet growth process will be controlled by thermal resistance between the droplet surface and the surrounding vapor:

$$\left.\frac{dr}{dt}\right|_{CON} = \frac{1}{\rho_l}\frac{\lambda_v}{r}\left(\frac{T_{sat} - T_v}{h_{lv}}\right) \tag{30}$$

where T_{sat} is the saturation temperature and λ_v is the vapor thermal conductivity. In Eq. (30) the term (T_{sat}–T_v) is known as subcooling level (T_{sub}) which results from non-equilibrium condition of the mixture. In order to determine the droplet growth in the entire range of varying Knudsen numbers, an interpolation which combines the relations for the free-molecular and continuum regimes is applied as follows [14]:

$$\frac{1}{\frac{dr}{dt}} = \frac{1}{\left.\frac{dr}{dt}\right|_{HK}} + \frac{1}{\left.\frac{dr}{dt}\right|_{CON}} \tag{31}$$

In the presented model, the phase change is represented by two mass sources as follows:

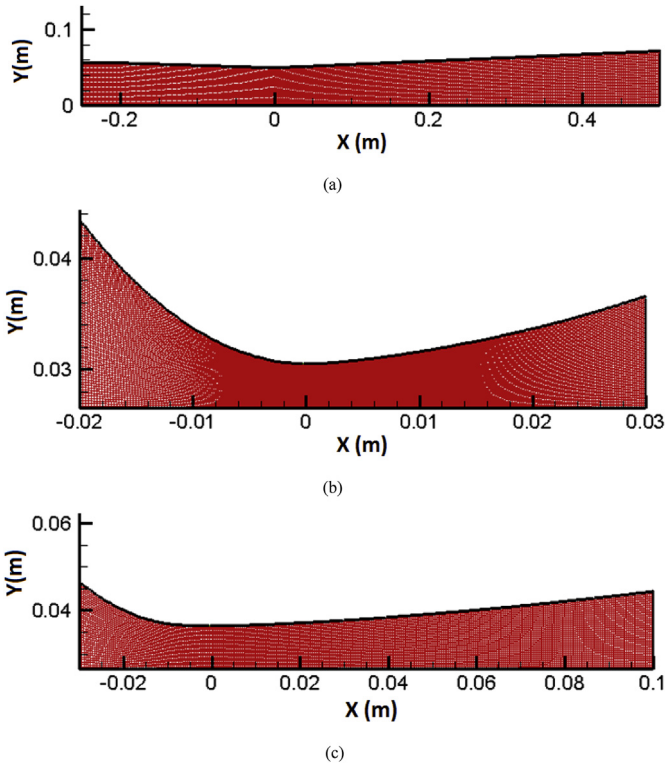

Fig. 1. Geometry of 3-dimensional (a) nozzle A, (b) nozzle 4/B, (c) nozzle 2/M.

$$\Gamma_1 = \frac{4}{3}\pi\rho_l r^{*3} J$$
$$\Gamma_2 = 4\pi\rho_l\rho_m n r^2 \frac{dr}{dt} \quad (32)$$

where Γ_1 and Γ_2 represent the mass sources due to creation of critical droplets in the nucleation process and condensation rate of all droplets per unit volume of the two-phase mixture, respectively. For calculating of the droplets radius, three additional transport equations for the moments according to Hill [6] are considered as follows:

$$\frac{\partial(\rho_l n)}{\partial t} + \frac{\partial\left(\rho_l n u_{lj}\right)}{\partial x_j} = J \quad (33)$$

$$\frac{\partial(\rho_l r)}{\partial t} + \frac{\partial\left(\rho_l r u_{lj}\right)}{\partial x_j} = r^* J + \frac{dr}{dt}\rho n \quad (34)$$

Table 2
Operating conditions for low-pressure and high-pressure nozzles.

	High-pressure nozzles		Low-pressure nozzle
Case	Nozzle 4/B- Case 18B	Nozzle 2/M- Case 40D	Nozzle A
Inlet total pressure (MPa)	10.07	10.09	0.025
Inlet total temperature (K)	638.7	637.5	354.6

$$\frac{\partial(\rho_l(r^2))}{\partial t} + \frac{\partial\left(\rho_l(r^2)u_{lj}\right)}{\partial x_j} = r^{*2} J + 2\frac{dr}{dt}\rho r \quad (35)$$

where n is number of droplets per unit kilogram of liquid phase. The average droplet radius is then calculated as:

$$r = \sqrt{\frac{(r^2)}{n}} \quad (36)$$

In this study, an in-house CFD code based on finite volume method is used for the simulation. Two-fluid multiphase formations are also implemented in the code. In addition to solving separate governing equations for each phase, phase interactions (mass transfer, interphase forces, drag forces, interphase heat transfer) are computed in the CFD code. A coupled, implicit and second order discretization scheme is used to improve the accuracy of the solution. Also the convergence criterion is set to 10^{-5} kg/s for the net mass flow rate within the computational domain. The following assumptions are considered for the numerical simulation:

1. The two phases have the same average pressure.
2. The computational domain of the thermo-compressor is assumed to be two dimensional and axisymmetric.
3. The flow regime is considered to be transient and turbulent.
4. Two separate governing equations are solved for each phase.
5. The steam and water properties are calculated based on the IAPWS-IF97 standard formulations [22].

3. Results and discussion

For the validation of the numerical simulations, the experiments of the nozzle flows with both low and very high inlet pressures are chosen. For low pressure nozzle, Moore et al. [11] nozzle A is chosen. For the very high pressure nozzle the flow through the Gyarmathy [26] nozzles 2/M and 4/B are chosen. The geometries of the simulated nozzles, 2/M and 4/B, are illustrated in Fig. 1. Also the detailed position of the nozzles surfaces are presented in Table 1. To obtain an optimal computational mesh, Grid Convergence Index

Table 1
Values of X and Y for the nozzles geometries.

(a) Nozzle A (width = 52 mm)													
X (m)			−0.25				−0.20				0.0		0.5
Y (m)			0.03785				0.03785				0.0315		0.057
(b) Nozzle 4/B (width = 20 mm)													
X (mm)	−20.00	−16.00	−12.00	−8.00	−4.00	0.00	4.00	8.00	12.00	16.00	20.00	24.00	28.00	30.00
Y (mm)	9.59	14.24	17.85	20.44	21.98	22.50	22.23	21.71	21.05	20.26	19.34	18.28	17.07	16.40
(c) Nozzle 2/M (width = 10 mm)													
X (mm)	−30.00	−24.00	−18.00	−12.00	−6.00	0.00	10.00	16.00	22.00	28.00	40.00	54.00	70.00	100.00
Y (mm)	6.51	10.79	13.85	15.69	16.37	16.50	16.29	16.04	15.73	15.37	14.53	13.40	11.92	8.59

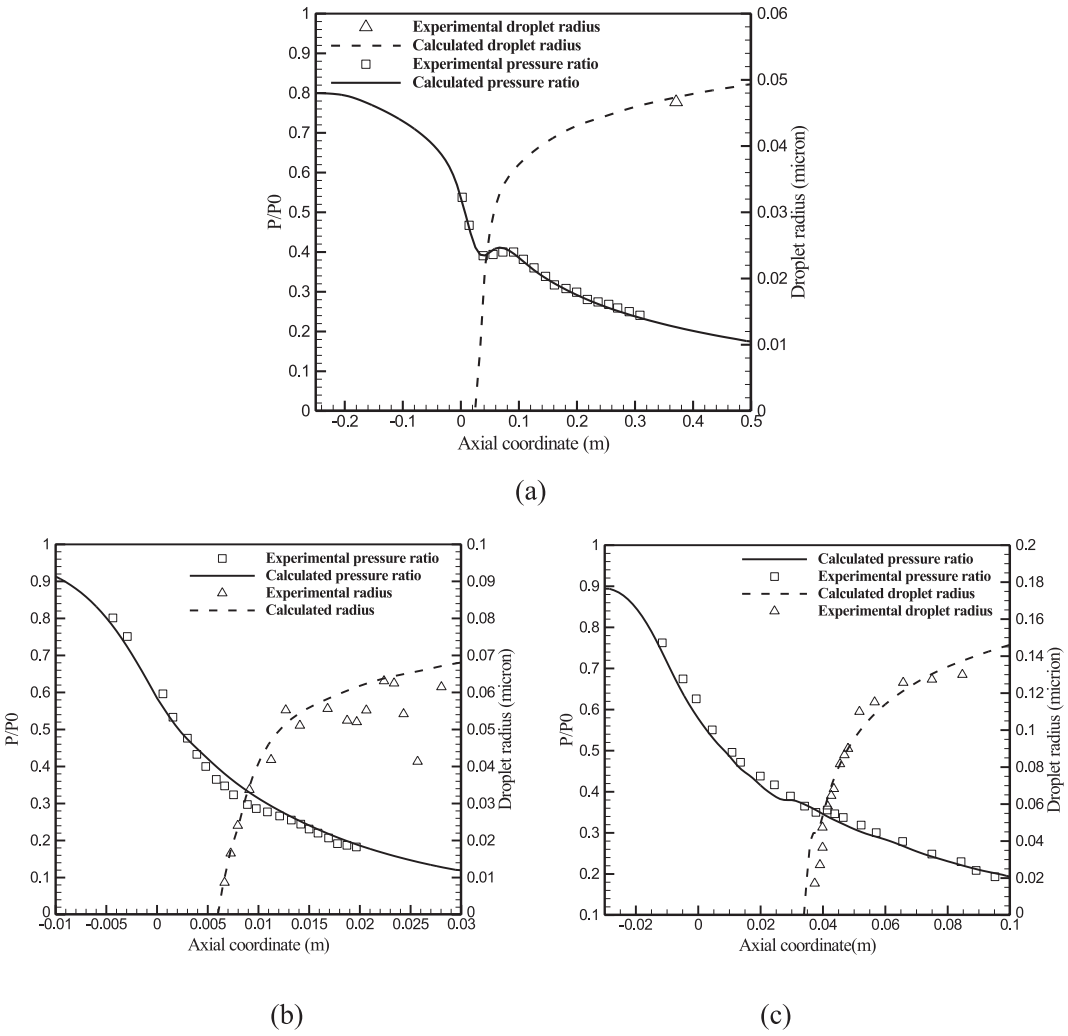

Fig. 2. Static pressure ratio and droplet radius distributions along axis of (a) nozzle A (Moore et al. [11]), (b) nozzle 4/B (Gyarmathy [26]), (c) nozzle 2/M (Gyarmathy [26]).

(GCI) [27] method is used to determine the appropriate grid resolution. For low-pressure nozzle Quadrilateral grids with 81 × 10 is used. Also quadrilateral grids with 401 × 60 and 301 × 60 nodes are used for high-pressure nozzles 2/M and 4/B, respectively. The operating conditions of the low and high pressure nozzles are presented in Table 2.

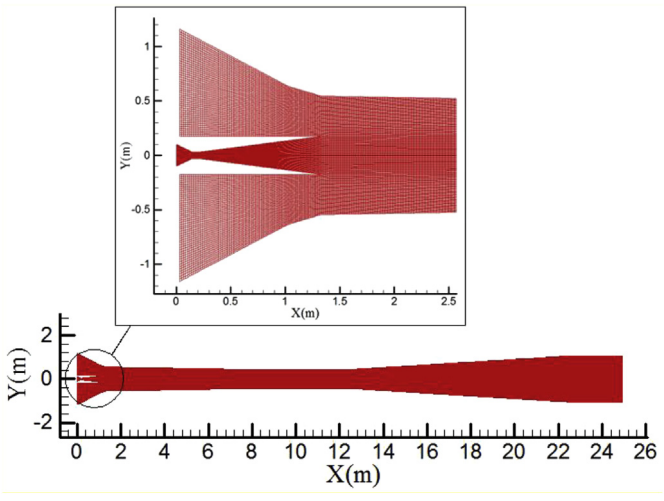

Fig. 3. Geometry of axisymmetric industrial high-pressure thermo-compressor.

Predictions of nozzle center line pressure and droplet radius for low and high pressure nozzles are compared with experiment in Fig. 2. As shown in Fig. 2, the calculated results for both low and high pressure cases have good agreement with experimental data. As it can be seen in Fig. 2(b)–(c), the maximum deviation for droplet radius calculation is about 0.01 microns for high-pressure nozzles.

In this study, the main focus is on the simulation of high-pressure thermo-compressors with the proposed two-fluid model. The geometry of the industrial thermo-compressor which is designed and manufactured by FAN NIROO Desalination and Water Solution Company [28] is illustrated in Fig. 3. A quadrilateral grid with 158700 cells is used after grid dependency study. It is attempted to use the grid sizes in the nozzle region similar to the

Table 3
Operating conditions for high-pressure thermo-compressor.

	Temperature (K)	Pressure (MPa)
Motive flow	553.15	3.4
Suction flow	321.15	0.0112
Discharge flow	341.75	0.0255

Table 4
Calculated mass flow rates and performance parameters of the simulated high-pressure thermo-compressor.

	Present study	Industrial data [28]	Error (%)
Motive flow (kg/s)	11.31	10.84	4.2%
Suction flow (kg/s)	14.02	14.2	−1.4%
Entrainment ratio	1.241	1.31	−5.4%
Compression ratio	2.27	2.276	0.0%

high-pressure nozzles. To achieve this purpose, the values of y^+ (dimensionless distance from wall) [19] for all walls of the thermo-compressor are set to be near 1.0. The operating conditions for the mentioned thermo-compressors are presented in Table 3.

Two main parameters which are defined for the performance analysis of a thermo-compressor are entrainment ratio and compression ratio. Entrainment ratio (ER) is defined as the ratio of secondary mass flow rate to the primary one ($m_{suction}/m_{motive}$) and compression ratio (CR) is defined as the ratio of discharge pressure to the suction pressure ($p_{discharge}/p_{suction}$).

The calculated mass flow rates for different boundaries of the thermo-compressor are presented in Table 4. As can be seen in Table 4, the calculated results can predict the performance parameters of thermo-compressors, successfully.

Fig. 4 shows the static pressure distributions along the centerline of the thermo-compressor. As depicted in Fig. 4 (a), the static pressure decreases along the nozzle and experiences a sudden

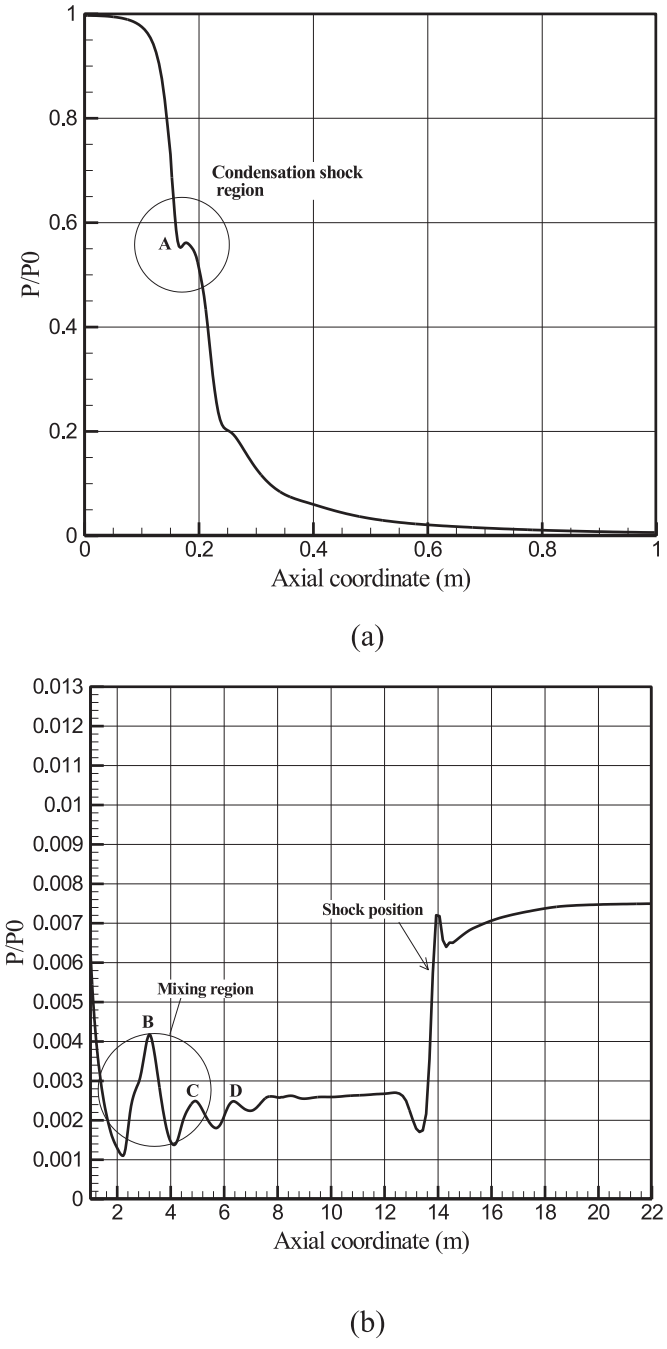

Fig. 4. Pressure distribution along the axis of thermo-compressor from (a) x = 0 m to x = 1 m and (b) x = 1 m to x = 22 m.

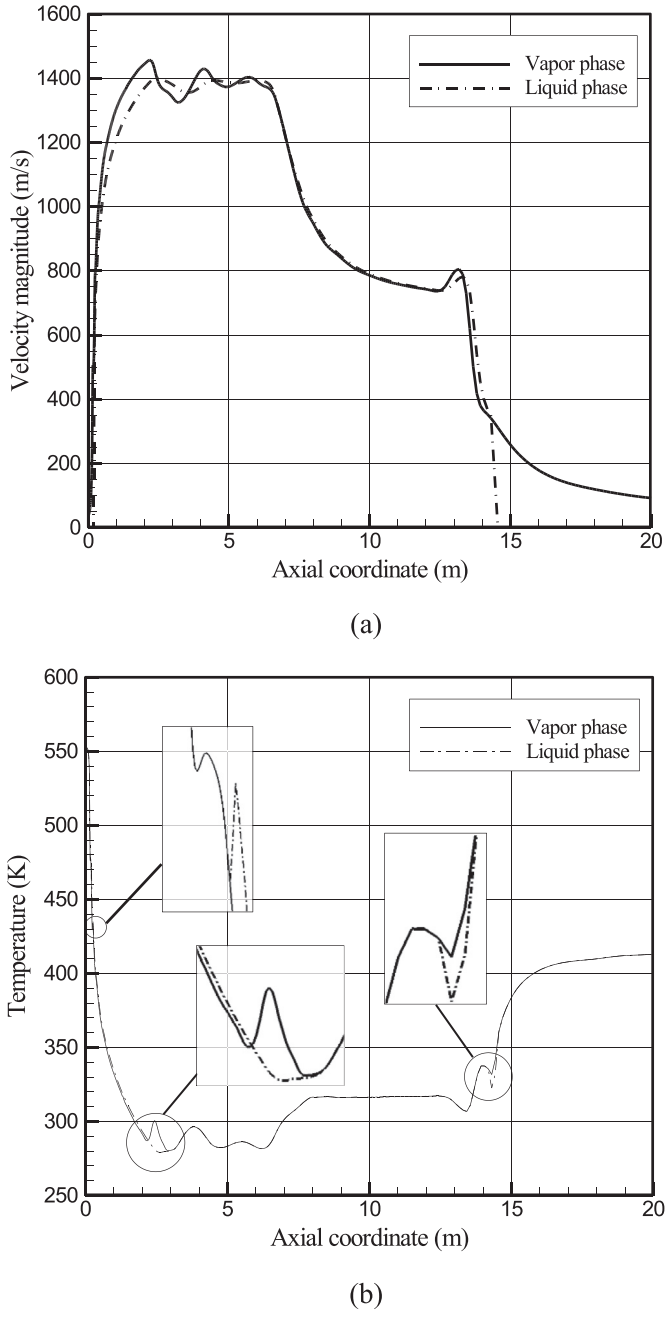

Fig. 5. Variations of (a) velocity and (b) temperature for each phase along the axis of thermo-compressor.

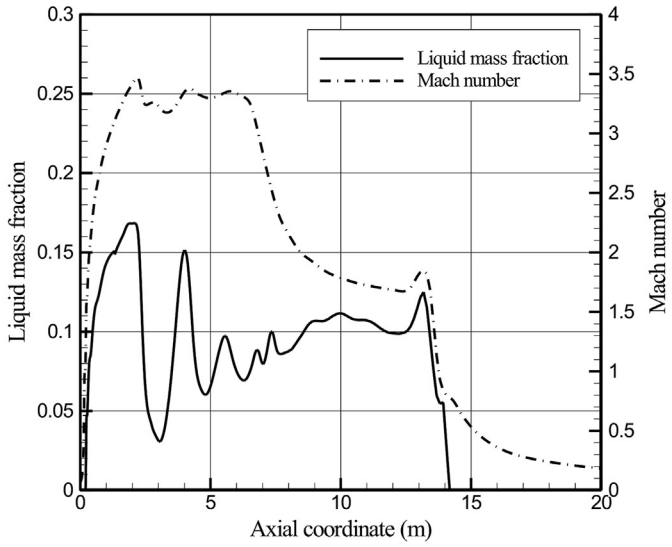

(a)

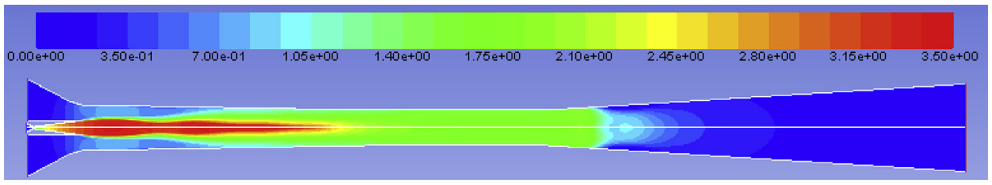

(b)

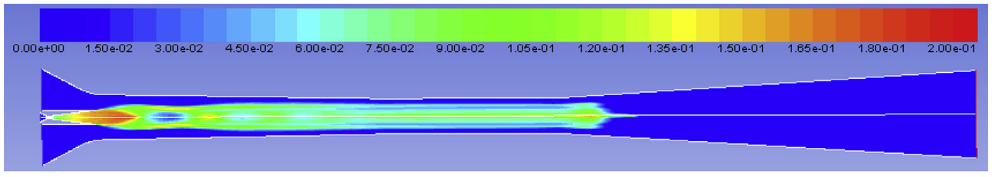

(c)

Fig. 6. Variations of (a) Mach number and mass fraction profiles along the axis of the thermo-compressor (b) contours of Mach number (c) contours of mass fraction.

increase when the non-equilibrium condensation happens which is known as condensation shock (point A). At the nozzle exit section, the primary fluid with the greater static pressure that secondary fluid enters the mixing region. Therefore, the shock train phenomenon can be observed through the fluctuation of static pressure at the centerline of the thermo-compressor (Fig. 4 (b)). The occurrence of a diamond wave jet core in the mixing tube indicates partial-separation of high-speed primary flow and the surrounding secondary fluid [29]. The static pressure keeps decreasing up to the diffuser section of thermo-compressor. At this section, a normal shock happens which cause a sudden jump in static pressure. Then the static pressure decrease smoothly to the discharge section of thermo-compressor.

Velocity and temperature distributions of vapor and liquid phases along the axis of the thermo-compressor are shown in Fig. 5. As it can be seen, when condensation happens and the liquid phase is produced, the formed droplets move at a lower velocity than vapor phase due to higher density (Fig. 5 (a)). At the diffuser section of thermo-compressor, the liquid phase vanishes completely. At this region, the mass of each droplet becomes very low and due to occurrence of dynamic shock in vapor phase which results in decrease of vapor velocity, the liquid velocity excels the vapor velocity. Due to release of latent heat, the droplets become hotter than the surrounding vapor during rapid non-equilibrium condensation. While the vapor and liquid phases reach to equilibrium state, the temperature difference between each phase diminishes (Fig. 5 (b)).

Variations of liquid mass fraction and Mach number along the axis of the thermo-compressor are illustrated in Fig. 6. Due to occurring of condensation in the diffuser section of the nozzle the liquid mass fraction increases rapidly to a peak value of 0.17 (Fig. 6 (a)). At the mixing region, when the supersonic flow of steam passes through the converging section of the thermo-compressor casing, the static pressure decreases which results in occurrence of nucleation process for the second time (points B, C and D in Fig. 4 (b)). As a results a second peak value for the liquid mass fraction can be seen at $x = 4$ m. The basic design of the simulated thermo-compressor is so that it works in double-choked condition. Therefore the Mach number in constant area of nozzle and thermo-compressor casing should reach to unity. Mach number along the axis of the thermo-compressor increases rapidly in nozzle region and then decreasing within the mixing region and constant area section of thermo-compressor casing. At the diffuser section of the thermo-compressor, due to occurrence of a shock, Mach number

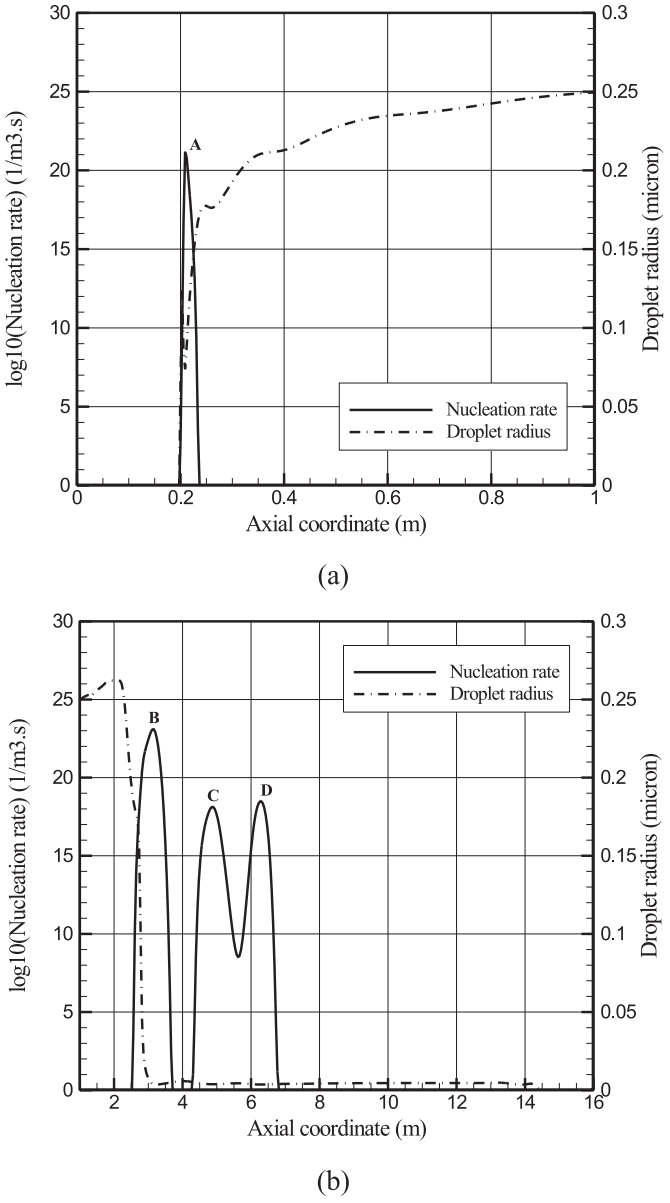

Fig. 7. Variations of nucleation rate and radius of produced droplets along the axis of thermo-compressor from (a) x = 0 m to x = 1 m and (b) x = 1 m to x = 16 m.

falls below unity (Fig. 6 (b)). Also at this point the due to increase of vapor pressure and temperature the liquid phase vanishes completely (Fig. 6 (c)).

The distributions of the nucleation rate and droplet radius are presented in Fig. 7. At the diffuser region of the nozzle the nucleation rate increases dramatically (Fig. 7 (a)). With production of liquid droplets the average droplet radius increases, consequently. Due to large motive pressure of thermo-compressor the radius of produced droplet becomes as large as 0.25 microns and therefore the volume fraction of the liquid phase cannot be neglected. As discussed above, although the second nucleation process happens in the mixing region (points B, C and D in Fig. 7 (b)) the radius of the droplets does not increase similar to the nozzle diffuser. It is due to the fact that the static pressure of the steam is smaller than that of nozzle diffuser.

The distribution of the number of droplets is presented in Fig. 8. As it can be seen, at the points of maximum nucleation rate (points

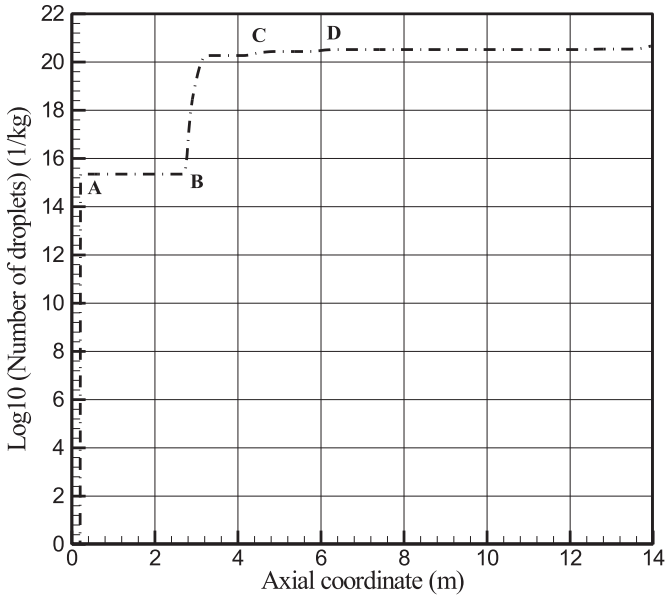

Fig. 8. Variations of number of produced droplets along the axis of thermo-compressor.

A, B, C and D) the number of droplets increases and becomes constant when nucleation processes end. The increase in number of droplets due to the secondary nucleation process is higher than that of the primary one. It is due to the fact that, each droplet which is produced in primary nucleation process acts as nuclei and increases the rate of droplet production phenomenon.

4. Conclusion

In this study, two-fluid multiphase formulations are applied for the prediction of non-equilibrium condensation of wet steam flow within industrial high-pressure thermo-compressor. Theory of non-equilibrium condensation of wet steam as well as suitable equations of state for both vapor and liquid phase are used via in-house CFD code. Quantitative validation of simulated results with experimental and industrial data shows that the present two-fluid model can predict the non-equilibrium condensation phenomena of high-pressure steam flow. Within the numerical investigation, the following conclusions are made:

1. The proposed two-fluid multiphase flow formulations can predict flow structure and non-equilibrium condensation phenomenon within high-pressure nozzle, successfully.
2. At high pressures of motive steam in thermo-compressors, due to production of high mass fraction of liquid phase the slip velocity and temperature difference between vapor and liquid phase cannot be neglected. Therefore the traditional wet-steam or single-fluid models in which the effects of liquid phase volume fraction and slip velocity are ignored are not further valid.
3. The second nucleation process occurs in the mixing region of the thermo-compressor at lower pressure than that of the nozzle diffuser region. As a result, the liquid mass fraction and number of produced droplets are increased.
4. It is observed that in the diffuser region of the thermo-compressor casing the liquid phase velocity excels the vapor phase velocity due occurrence of normal shock. The same phenomenon in the mixing region can be seen due to pressure fluctuations.

5. The results showed that droplet production due to secondary nucleation process in much larger than that of primary nucleation process.

Nomenclature

CR	compression ratio
E	total energy (J)
ER	entrainment ratio
F_D	drag forces (N)
H	total enthalpy (J/kg)
h	enthalpy (J/kg)
h_c	heat transfer coefficient ($W/m^2.k$)
J	nucleation rate ($1/m^3.s$)
K	turbulent kinetic energy (m^2/s^2)
Kn	Knudsen number
M	mass of one molecule of water (kg)
n	number of droplet per unit mass of vapor (#1/kg)
P	pressure (Pa)
Pr	Prantdl number
r	droplet radius (m)
R	gas constant (J/kg.K)
t	time (s)
T	temperature (K)
u	velocity (m/s)
x	direction (m)

Greek symbols

λ	thermal conductivity (W/m.K)
σ	surface tension (N/m)
Γ	mass transfer rate ($kg/m^3.s$)
α	liquid volume fraction
τ	stress tensor (N/m^2)
ρ	density (kg/m^3)
ε	turbulent dissipation rate (m^2/s^3)
l	free molecular pass (m)
μ	viscosity (Pa.s)

Subscript:

int	interface
l	liquid
lv	liquid-vapor
m	mixture
q	vapor or liquid phase
sat	saturation
sub	subcooling level
v	vapor

References

[1] M. Ji, T. Utomob, J. Woo, Y. Lee, H. Jeong, Ha Chung, CFD investigation on the flow structure inside thermo vapor compressor, Energy 35 (2010) 2694–2702.

[2] R. Kouhikamali, N. Sharifi, Experience of modification of thermo-compressors in multiple effects desalination plants in Assaluyeh in IRAN, App. Therm. Eng. 40 (2012) 174–180.

[3] N. Sharifi, M. Boroomand, R. Kouhikamali, Wet steam flow energy analysis within thermo-compressors, Energy 47 (2012) 609–619.

[4] A.D. Gosman, E. Ioannides, Aspect of computer simulation of liquid fuelled combustion, in: AIAA 19th Aerospace Science Meeting, McGraw Hill, St Louis, 1981, pp. 1285–1293.

[5] X.F. Yu, A Numerical Simulation of Wet Steam Flow Based on Dual Fluid Model, Dissertation for the Master Degree in Engineering in Harbin Institute of Technology, 2011, p. 16.

[6] P.G. Hill, Condensation of water vapor during supersonic expansion in nozzles, J. Fluid. Mech. 25 (1966) 593–620.

[7] J.B. Young, The spontaneous condensation of steam in supersonic nozzles, Phys. Chem. Hydrodyn. 3 (1982) 57–82.

[8] G. Gyarmath, On the growth rate of droplets in a supersaturated atmosphere, Math. Phys. 14 (1963) 280–293.

[9] F. Bakhtar, K. Zidi, On the self-diffusion of water vapor, Proc. Inst. Mech. Eng. Part C 199 (1985) 159–164.

[10] A.G. Gerber, M.J. Kermani, A pressure based Eulerian- Eulerian multi-phase model for non-equilibrium condensation in transonic steam flow, Int. J. Heat. Mass Transf. 47 (2004) 2217–2231.

[11] M.J. Moore, P.T. Walters, R.I. Crane, B.J. Davidson, Predicting the fog drop size in wet steam turbines, Institute of Mechanical Engineers (UK), in: Wet Steam 4 Conf, University of Warwick, 1973 paper C37/73.

[12] S. Dykas, W. Wroblewski, Two-fluid model for prediction of wet steam transonic flow, Int. J. Heat. Mass Transf. 60 (2013) 88–94.

[13] H. Ding, C. Wang, C. Chen, Non-equilibrium condensation of water vapor in sonic nozzle, Appl. Therm. Eng. 71 (2014) 324–334.

[14] A.R. Avetissian, G.A. Philippov, L.I. Zaichik, Effects of turbulence and inlet moisture on two-phase spontaneously condensing flows in transonic nozzles, Int. J. Heat. Mass Transf. 51 (2008) 4195–4203.

[15] A.R. Avetissian, G.A. Philippov, L.I. Zaichik, The effect of turbulence on spontaneously condensing wet-steam flow, Nucl. Eng. Des. 235 (2005) 1215–1223.

[16] S. Dykas, W. Wroblewski, Single- and two-fluid models for steam condensing flow modeling, Int. J. Multi. Flow. 37 (2011) 1245–1253.

[17] J. Feng-ming, Y. Pei-gang, H. Wan-jin, Numerical investigation on wet steam non-equilibrium condensation flow in turbine Cascade, J. Therm. Sci. 21 (2012) 525–532.

[18] K. Cui, H. Chen, Y. Song, H. Oyama, Research on wet steam spontaneous condensing flows considering phase transition and slip, J. Therm. Sci. 22 (2013) 320–326.

[19] Z. Yang, T.H. Shih, New time scale based k-ε model for near wall turbulence, AIAA J. 7 (1993) 1191–1197.

[20] C.G. Speziale, On nonlinear k-l and k-ε models of turbulence, J. Fluid Mech. 178 (1987) 459–475.

[21] T.B. Gatski, C.G. Speziale, On explicit algebraic stress models for complex turbulent flows, J. Fluid Mech. 254 (1993) 59–78.

[22] W. Wagner, The IAPWS industrial formulation 1997 for the thermodynamic properties of water and steam, Trans. ASME J. Eng. Gas Turbines Power 122 (2000).

[23] K. Oswatitsch, Kondensationserscheinungen in überschalldüsen, J. Appl. Math. Mech. Z. Angew. Math. Mech. 22 (1942) 1–14.

[24] M.E. Deich, V.F. Stepanchuk, G.A. Saltanov, Calculating of the Rate of Formation of Condensation Centers in Supersaturated Vapor, Heat Transfer – Soviet, Research I, vol. 2, 1969, pp. 106–111.

[25] J. Young, The condensation and evaporation of liquid droplets at arbitrary Knudsen number in the presence of an inert gas, Int. J. Heat. Mass Transf. 36 (1993) 2941–2956.

[26] G. Gyarmathy, Nucleation of steam in high-pressure nozzle experiments, Proc. IMechE Part A: J. Power Energy 219 (2005) 511–521.

[27] P.J. Roache, Verification and validation in computational science and engineering, Comput. Sci. Eng 1 (1998) 8–9.

[28] http://www.fanniroogroup.com/.

[29] Y. Bartosiewicz, Z. Aidoun, P. Desevaux, Y. Mercadier, Numerical and experimental investigations on supersonic ejectors, Int. J. Heat Fluid Flow 26 (2005) 56–70.